Astron. Astrophys. 261, 25–40 (1992)

ASTRONOMY AND ASTROPHYSICS

The radio structure of extended quasars

II. The radio emission on pc- and kpc-scales

J.R.A. Hooimeyer[1], R.T. Schilizzi[1,2], G.K. Miley[1], and P.D. Barthel[3]

[1] Leiden Observatory, P.O. Box 9513, NL-2300 RA Leiden, The Netherlands
[2] Netherlands Foundation for Research in Astronomy, P.O. Box 2, NL-7990 RA Dwingeloo, The Netherlands
[3] Kapteyn Astronomical Institute, University of Groningen, P.O. Box 800, NL-9700 AV Groningen, The Netherlands

Received September 19, 1991; accepted January 27, 1992

Abstract. VLBI and VLA observations of the nuclear and overall radio structures are presented for eight quasars possessing large double-lobed radio emission. On milli-arcsec scales, the nuclei of five sources show an asymmetric (core–jet) morphology, one has a symmetric appearance, one is unresolved and one is too weak to allow a reliable determination of its structure. Total intensity, polarization and spectral index maps of the associated kpc-scale emission were obtained for six of the eight quasars. The inner and outer radio jet emission generally are well aligned and pointing in the same direction; in one source, the pc- and kpc-scale jet are oppositely directed. Jet velocities close to the hot spots were estimated for several quasars from the intensity of their hot spot emission. The velocity estimates were relativistic in all cases (ranging from 0.5 to 0.9 c).

Key words: interferometry – quasars: general – radio sources: general

1. Introduction

Powerful radio sources show a great diversity in radio morphology and spectral behaviour. The well-known relativistic beaming model (Blandford & Königl 1979; Scheuer & Readhead 1979; Orr & Browne 1982) has proven remarkably successful in explaining this variety of observational characteristics in terms of the orientation of relativistically expanding jet material. The mapping and monitoring of the milliarcsec (mas) scale emission in the nuclei of large lobe-dominated sources has long been considered to provide a vital observational test to the beaming hypothesis (e.g. Scheuer 1984). Since, within the context of the beaming model, these objects are hypothesized to lie in or close to the plane of the sky, their core emission should exhibit symmetrical (not one-sided) structure, and subluminal, or at best mildly superluminal, expansion. Detection of significant superluminal motion or systematically asymmetric nuclear radio structure in a large fraction of lobe-dominated sources should present strong evidence against the simple Orr and Browne model. This idea triggered the setup of several very long baseline interferometry (VLBI) monitoring projects of large samples of lobe-dominated sources.

Since the early eighties, our group has been involved in studying the radio characteristics of a sample of 30 quasars with large double-lobed structure. These sources were selected from the optical QSO catalogue of Hewitt & Burbidge (1980) on the basis of their angular radio extent and their nuclear radio luminosity. We chose to concentrate on extended quasars with bright radio cores, rather than on a randomly oriented sample of objects including many weak nuclei; this allowed us to obtain mas-scale structural information for a complete sample of double-lobed quasars within a limited amount of observing time. The large physical sizes of the selected sources should help ensure that they are oriented at large angles to the line of sight (see discussion in Hooimeyer et al. 1991; henceforth HBSM).

A preliminary VLBI survey, the results of which have been described in Barthel et al. (1984) and HBSM, yielded evidence for the presence of resolved structure on mas scales in 13 of the 30 sources. Two of these, the quasars 1137+660 (3C 263) and 1150+497 (4C 49.22) have been studied by other investigators (Zensus & Porcas 1986; Linfield, unpublished). The remaining 11 sources have been observed by us with global VLBI networks at 5 GHz. For three of the 11 quasars, the sources 0610+260, 0742+318 and 1721+343, observations have already been published elsewhere (Barthel et al. 1985, 1989). First-epoch VLBI maps of the remaining eight sources will be presented and discussed in this article. For six of these sources, additional observations of the associated large scale radio structure have been obtained at 5 and 15 GHz with the very large array (VLA; Thompson et al. 1980). Section 2 describes the observations and the data reduction. In Sect. 3, the VLBI and VLA data are presented and discussed for each quasar individually. Subsequently, a comparison is made between the morphologies of the pc-scale nuclear structure (presumed to be due to recent activity) and the overall morphology of the extended quasars (produced by integrated activity over 10^7 yr). This should give us a better insight in the evolution of the radio jets in these large objects. An estimate of jet velocities in extended quasars close to the radio lobes can be obtained from the luminosity and energy density of the hot spot emission. In Sect. 5, jet velocities in the vicinity of the lobes are estimated for several extended quasars. Finally, in Sect. 6 the most relevant results are summarized, and their implications discussed briefly.

Send offprint requests to: G.K. Miley

2. Observations and data reduction

2.1. VLBI observations

At 5 GHz, the nuclei of all eight extended quasars could be mapped using the Mk II recording system. Observations of the eight quasars have been made with global VLBI networks at 5 GHz during the period 1985–1988. A journal of the observations is shown in Table 1. The quantity and quality of the data varied considerably. For five quasars (0850+581, 1317+520, 1548+114, 1830+285, 2251+134) a full 12 h coverage could be obtained; for the sources 1055+201, 1222+216 and 2209+080 the observing runs were of shorter duration. Source switching was applied between 1055+201 and 1222+216.

All experiments were carried out using standard Mk II recording equipment at 2 MHz bandwidth. Left circular polarization was recorded. The data were correlated using the 5- and 10-stations Mk II correlators at the California Institute of Technology (Caltech) in Pasadena, and then coherently averaged over 2–4 min. For the weakest objects, 2209+080, 1548+114 and 1830+285, global fringe fitting was applied (Schwab & Cotton 1983). The correlated data were reduced using the Caltech VLBI and AIPS software packages. Flux calibration was performed following Cohen et al. (1975), assuming the primary calibrators to be unresolved on all baselines. The usual self-calibration and hybrid mapping procedures were applied (e.g. Pearson & Readhead 1984). An overview of the derived model parameters is presented in Table 2. The values quoted for component flux, separation and position angle represent a weighted mean of the values determined by the model fitting and hybrid mapping procedures. Errors in these numbers have been estimated by visual inspection and reduced χ^2 values for the agreement between model and observed visibilities.

2.2. VLA observations

Low-frequency radio maps of arcsec resolution (at 1400 and 408 MHz) of the eight quasars which we have studied with VLBI, have been published by Hintzen et al. (1983), Owen & Puschell (1984), and Shone (1985). Our objective was to obtain supplementary high signal-to-noise maps of these sources at higher frequency and resolution. For two of the eight quasars, detailed VLA and MERLIN maps of high quality have been made by other observers: 0850+581 (Shone 1985) and 1222+216 (Neff, private communications). The remaining six objects have been mapped by ourselves with the VLA in its B-configuration at 5 and 15 GHz, and a bandwidth of 50 MHz. The resolution achieved at these frequencies is $\sim$1 and 0.3″, respectively. Total intensity (I) and linear polarization (P) maps were derived for all sources at both frequencies.

The observations were carried out in August 1986 in snapshot mode; two or three scans of $\sim$15 min duration each were taken of each object at various hour angles. Every source scan was preceded and succeeded by a short ($\sim$1–2 min) observation of a nearby secondary calibrator source. An absolute flux density level was established using several short observations of the primary VLA flux calibrator 3C 48. Calibration of the instrumental polarization was achieved by repeated observation of 3C 286 at various parallactic angles. Atmospheric disturbances due to a local thunderstorm affected some of the 15 GHz scans. A sufficient amount of data was left to derive high signal-to-noise intensity maps for all six objects, but the noise in the 15 GHz polarization maps is relatively high.

The data were reduced using the standard AIPS reduction software. For each source, maps of the four Stokes parameters I, Q, U and V were obtained at 5 and 15 GHz. From these, maps of the spectral index α_5^{15}, the linear polarized intensity P, and the distribution of the electric vector ϕ were derived. The integrated flux densities, linear polarizations and polarization position angles are given for all quasars in Table 3. Table 3 further contains several morphological parameters of the large-scale radio emission, such as the angular extent, the jet–counterjet flux density ratio f and the jet–counterjet length asymmetry A. (A has been defined as $(E_1-E_2)/(E_1+E_2)$, where E_1 and E_2 are the distances from the quasar core to the farthest and nearest hot spot or lobe centroid, respectively.)

Flux densities, linear polarization levels and spectral index values were also determined for the main substructures in each source: core, jet, lobe and hot spots. These values are listed in

Table 1. Observing log

Source	Other name	VLA		VLBI		
		Observed date	Frequency (GHz)	Observed date	Duration (h)	Telescope name
0850+580	4C 58.17	—	—	01/06/86	12	SBWL-KG
1055+201	4C 20.24	14/7/86	5.15	01/06/86	6	SBWL-KG
1222+216	4C 21.35	—	—	01/06/86	6	SBWL-KG
1317+520	4C 52.27	14/7/86	5.15	01/10/87	12	SBWLJ-G
1548+114	4C 11.50	14/7/86	5.15	25/09/87	12	SBWLJ-G
1830+285	4C 28.45	14/7/86	5.15	02/06/86	12	SBWL-KG
2209+080	4C 08.64	15/7/86	5.15	02/06/86	6	SBWL-KG
2251+134	4C 13.85	15/7/86	5.15	27/09/85	12	SBWLJ-K
				02/06/86[b]	6	SBWL-KG

[a] Abbreviations of station names: S = Onsala (26 m), B = Effelsberg (100 m), W = WSRT (14 × 25 m), L = Medicina (32 m), J = Jodrell Bank (76 m), K = Haystack (36 m), G = Green Bank (43 m), Y = VLA (27 × 25 m), O = Owens Valley (40 m).
[b] 2251+134 re-observed.

Table 2. Parameters of VLBI CLEAN model components

Source	Component	Flux (mJy)	Distance (mas)	Position angle (°)	Size (mas)
0850+581	A	638±2	0.0	0	0.4±0.1
	B	99±2	1.1±0.1	161±1	0.4±0.1
	C	7±1	4.1±0.1	140±1	1.1±0.1
	D	6±1	6.1±0.1	155±1	0.7±0.1
	E	5±1	12.2±0.1	146±3	2.3±0.1
1055±201	A	516±2	0.0	0	0.2±0.1
	B	75±4	2.2±0.1	−6±1	0.4±0.1
	C	85±4	2.1±0.1	174±1	0.7±0.1
1222±216	A	360±1	0.0	0	0.8±0.1
	B	18±1	3.3±0.1	−15±1	0.5±0.1
	C	7±1	7.2±0.1	−12±1	0.8±0.1
1317+520	A	108±2	0.0	0	0.8±0.1
	B	21±1	4.7±0.1	125±1	0.8±0.1
	C	8±1	6.1±0.1	126±1	0.8±0.1
	D	5±1	8.3±0.1	135±2	0.8±0.1
1548+114	A	310±1	0.0	0	0.3±0.1
	B	12±1	1.4±0.1	69±4	0.6±0.1
1830+285	A	312±1	0.0	0	0.6±0.1
	B	25±2	2.1±0.1	−37±1	0.5±0.1
	C	21±2	3.9±0.1	−33±1	0.5±0.1
2209+080	A	148±4	0.00	0	3×1
2251+134	A	370±2	0.0	0	0.5±0.1
	B	62±2	1.8±0.1	39±2	0.8±0.1
	C	54±1	2.5±0.1	−138±2	1.0±0.1

Table 3. Integrated radio parameters

Source	15 GHz		5 GHz				
	Flux (mJy)	% pol.	Flux (mJy)	% pol.	LAS[a] (″)	A[a]	f[b]
1055+201	862	0.7	1370	2.5	62	0.2	—/—
1317+520	245	1.3	491	11.2	29	0.3	4.6/24
1548+114	231	0.0	402	0.2	46	0.1	6.0/45
1830+285	482	1.8	780	4.1	28	0.0	6.0/35
2209+080	305	4.2	628	6.7	16	0.3	4.0/90
2251+134	792	0.0	948	2.9	13	0.3	1.5/—

[a] Measured from lowest frequency map.
[b] Quoted values of jet–counterjet flux density ratios for 5 and 15 GHz, respectively.

Table 4. Minimum energy densities u_{min} and equipartition magnetic field values B_{eq} were determined under the usual assumptions of cylindrical symmetry, energy equipartition between relativistic particles and the magnetic field, and a filling factor of unity (Miley 1980). The luminosity of the individual components has been calculated using $H_0 = 100h$ km s^{-1} Mpc^{-1} and $q_0 = 0.05$.

3. Notes on individual sources

3.1. 0850+581

This distorted triple radio source contains one of the brightest radio cores in our sample; strictly speaking, it is not a lobe-dominated object. Because of its high radio luminosity, 0850 +581 has been included in the bright source survey of Pearson &

Table 4. Derived parameters for source components

Component	S_5 (mJy)	% pol. P_5	S_{15} (mJy)	% pol. P_{15}	α_5^{15}	u_{min} (erg cm^{-3})	B_{eq} (G)
1055+201							
Core	1067	2.4	685	0.7	0.4	$6.7\,10^{-8}$	$8.3\,10^{-4}$
Jet	38	—	—	—	—	—	—
N lobe[a]	232	0.5	96	0.5	0.7	$1.7\,10^{-10}$	$0.4\,10^{-4}$
Hot spot	132	0.5	65	0.5	0.65	$9.9\,10^{-9}$	$4.4\,10^{-4}$
S lobe	35	—	—	—	—	$1.4\,10^{-10}$	$0.4\,10^{-4}$
1317+520							
Core	316	10.7	190	1.2	0.45	$3.2\,10^{-8}$	$5.7\,10^{-4}$
Jet	26	3.4	7	—	1.15	$1.6\,10^{-10}$	$0.4\,10^{-4}$
NW lobe	21	2.4	—	—	>2.0	$1.5\,10^{-11}$	$1.2\,10^{-5}$
SE lobe[a]	128	5.8	46	0.9	0.90	$1.2\,10^{-10}$	$3.5\,10^{-5}$
Hot spot	89	4.9	41	0.9	0.80	$0.9\,10^{-10}$	$3.2\,10^{-5}$
1548+114							
Core	339	<0.5	231	—	0.35	$1.5\,10^{-8}$	$3.9\,10^{-4}$
Jet	12	<0.5	—	—	—	$0.4\,10^{-10}$	$0.2\,10^{-4}$
SE lobe	5	<0.2	—	—	—	$1.7\,10^{-12}$	$4.2\,10^{-6}$
NW lobe[a]	48	<0.5	—	—	—	$5.1\,10^{-12}$	$7.2\,10^{-6}$
Hot spot	42	1.0	—	—	—	$4.0\,10^{-9}$	$2.0\,10^{-4}$
1830+285							
Core	592	—	423	—	0.30	$2.7\,10^{-8}$	$5.2\,10^{-4}$
Jet	31	—	12	—	0.85	$7.7\,10^{-11}$	$2.8\,10^{-5}$
SE lobe	35	—	10	—	1.15	$1.1\,10^{-10}$	$1.1\,10^{-5}$
NW lobe[a]	115	4.0	37	1.7	1.0	$3.0\,10^{-11}$	$1.8\,10^{-5}$
Hot spot	60	4.0	32	1.7	0.50	$2.4\,10^{-9}$	$2.6\,10^{-4}$
2209+080							
Core	235	5.8	190	1.2	0.20	$1.4\,10^{-8}$	$3.8\,10^{-4}$
N lobe	99	1.5	25	—	1.25	$1.3\,10^{-10}$	$3.5\,10^{-5}$
S jet	110	2.4	57	—	0.60	$0.3\,10^{-9}$	$5.5\,10^{-5}$
S lobe[a]	69	1.8	18	—	1.20	$1.8\,10^{-10}$	$4.3\,10^{-5}$
Hot spot	25	1.7	9	—	0.90	$0.9\,10^{-9}$	$1.8\,10^{-4}$
2251+134							
Core	648	4.7	730	—	−0.1	$3.6\,10^{-8}$	$6.0\,10^{-4}$
NE lobe+jet	137	—	25	0.8	1.5	$0.9\,10^{-10}$	$3.2\,10^{-5}$
SW jet	52	2.9	16	—	1.05	$7.3\,10^{-10}$	$8.7\,10^{-5}$
SW lobe	111	2.1	19	—	1.60	$3.4\,10^{-10}$	$5.8\,10^{-5}$

[a] Total lobe emission, including hot spot regions.

Readhead (1984), and as such it already had been observed with VLBI at several epochs, for a few hours at a time, prior to the present observations. It has since then been discovered to be a superluminal source (Barthel et al. 1986).

We have not obtained arcsec-resolution observations of this source. A high signal-to-noise MERLIN map of the large-scale radio structure of 0850+581 is shown in Shone (1985) and Browne (1987). Here we present VLBI observations of the nuclear emission of 0850+581.

At epoch 1986.42, 0850+581 was tracked by an 8-station network for a full 12 h. The resulting map is shown in Fig. 1a. The mas-scale radio structure is dominated by a bright northern component, containing approximately 85% of the total flux in the map. On the grounds of its relative brightness and its flux variability, we assume this component (designated A in Fig. 1) to be the quasar core. Secondary resolved components, B and C, are located at 4.4 and 6.3 mas to the southeast of A, and a weak resolved feature D is present at roughly 11 mas distance. The visibilities on the shortest baselines further indicate the presence of ~10 mJy of diffuse emission at distances of 20–30 mas from the core, beyond the boundaries of the man displayed in Fig. 1, and aligned along a position angle 178±4°. The three features B, C, and D were detected in the earlier maps of Barthel et al. (1986). In addition, a new component A′, close to the core, has become apparent, which was not present in previous maps; meanwhile, the central component A itself has decreased in flux density by ~15% compared to the value quoted by Barthel et al. for their last epoch 1985.77. The mas-scale structure is not perfectly collinear, and appears to "wiggle" on the scale of a few mas. The newly discovered component A′ is elongated along a position

angle of $174 \pm 4°$ with respect to the core A, whereas the more distant components B, C and D are resolved along position angles of 164 ± 2, 162 ± 2 and $168 \pm 3°$, respectively. On kpc scales the radio jet of 0850+581 displays a similar "cork–screw" behaviour (Barthel et al. 1986). The wiggle of the jet on mas and arcsec scales is consistent with an interpretation in terms of precession of the radio axis.

When compared with the data of Barthel et al., the 1986.42 map of 0850+581 confirms the presence of superluminal motion in this quasar. In Fig. 1b the distance of components B and C with respect to the core A is plotted versus time. A weighted least-squares fit through the data of the three epochs of Barthel et al. (1986) and the 1986.42 data yield a proper motion $\mu_{B,C} = 0.11 \pm 0.02$ mas yr^{-1}. At a redshift $z = 1.322$ and using $H_0 = 100h$, $q_0 = 0.05$, this value corresponds to an apparent expansion velocity $\beta_{app} = (4.8 \pm 0.7)h^{-1}c$, which is equal to within the errors to the value of $(5.3 \pm 0.8)h^{-1}c$ given by Barthel et al.

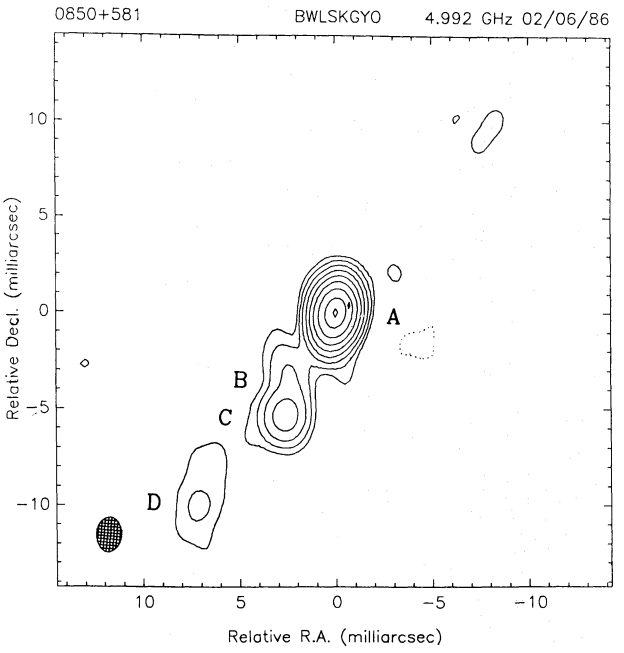

Fig. 1a. 5 GHz VLBI map of the total intensity I of 0850+581, observed at epoch 1986.42. The contour levels in the map are 0.2, 0.5, 1, 2, 4, 8, 16, 32, 64 and 96% of the peak flux value of 649 mJy per beam. The restoring beam is an ellipse of 1.8×1.2 mas, at a position angle of $-5°$

3.2. *1055+201*

(*a*) *Mas-scale radio structure*: In the earliest VLBI observations of this large double-lobed radio source (Barthel et al. 1984), the mas-scale nuclear emission was unresolved at 5 GHz, implying an angular core size smaller than 1 mas. In the middle of 1984, however, 1055+201 underwent a radio flare, in which the core brightened by approximately 50%. Subsequent VLBI snapshot observations indicated the nuclear radio emission to be resolved at 5 GHz, and roughly 4 mas in size (HBSM).

Figure 2a shows the map of the radio core of 1055+201 obtained in June 1986. The quality of these data was low. The experiment suffered from station failures and very poor tape playback performance. Also, source switching between 1055+201 and another source resulted in large gaps in the *uv*-coverage. The best fit to the visibilities was obtained by a triple structure 4×0.7 mas in size, oriented along a position angle of $-6°$ (i.e. in the direction of the northern radio lobe). The two outer features are both considerably weaker than the central component, and of roughly equal flux density.

Attempts during the mapping procedure to force the clean-component model towards an asymmetric mas-scale structure, resulted in appreciably worse fits of the model to the visibility amplitudes and phases. Also, the closure phases do not show any systematic offset from zero within the errors, which is further evidence that the symmetry in the map is real. However, the noise in the phase data is large on the weaker baselines, so that the possibility that the observed symmetry is an artifact caused by phase errors cannot be excluded.

(*b*) *Large-scale radio structure*: The large, double-lobed radio source associated to 1055+201 is dominated by a bright, flat

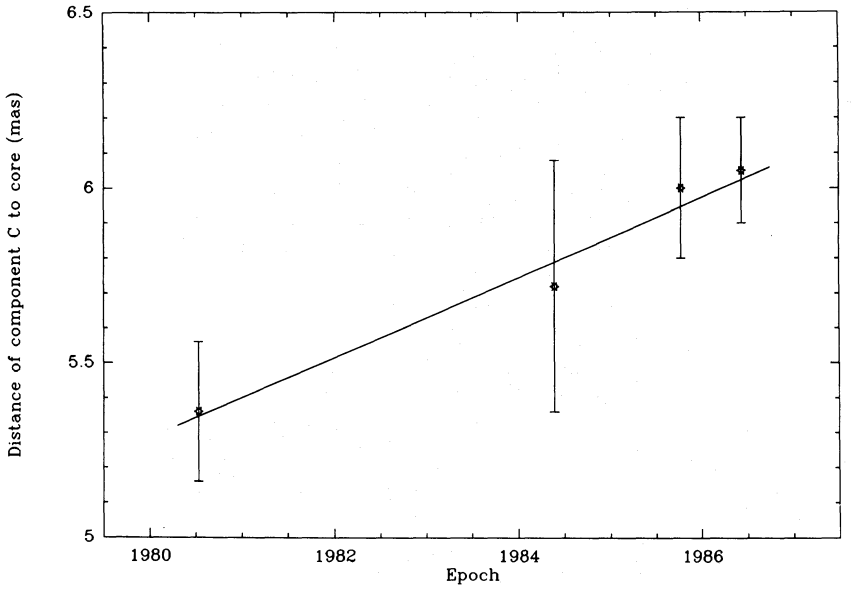

Fig. 1b. The distance of components B and C with respect to the presumed core A as function of time. Data points and error bars of the epochs preceding 1986.42 have been taken from Barthel et al. (1986); the data from epoch 1986.42 have been taken from the present map. The solid line represents a weighted least-squares fit through the data of component B, the dashed line the same for component C. The proper motions implied by the two fits are $\mu_B = 0.11 \pm 0.02$ and $\mu_C = 0.12 \pm 0.02$ mas yr^{-1}, respectively

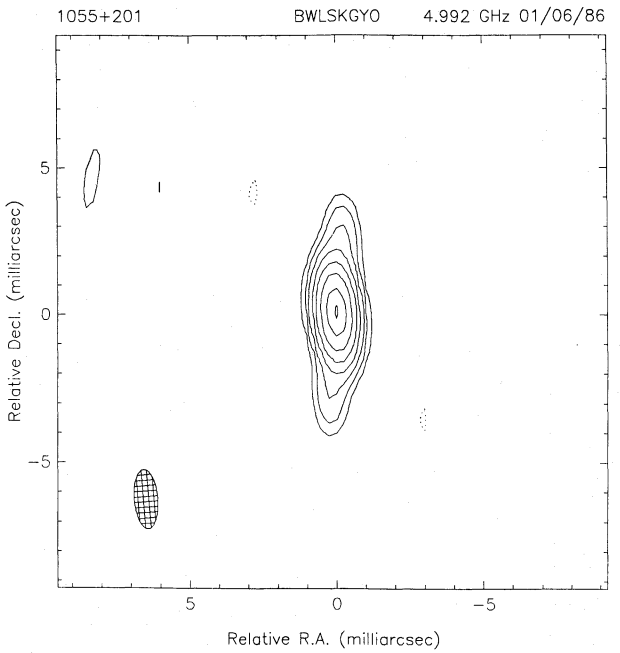

Fig. 2a. 5 GHz VLBI map of the total intensity I of 1055+201, observed at epoch 1986.42 in source switching mode with 1222+216. The contour levels in the map are 0.5, 1, 2, 4, 8, 16, 32, 64 and 96% of the peak flux value of 591 mJy per beam. The restoring beam is an ellipse of 2.0 by 1.0 mas, at a position angle of 8°

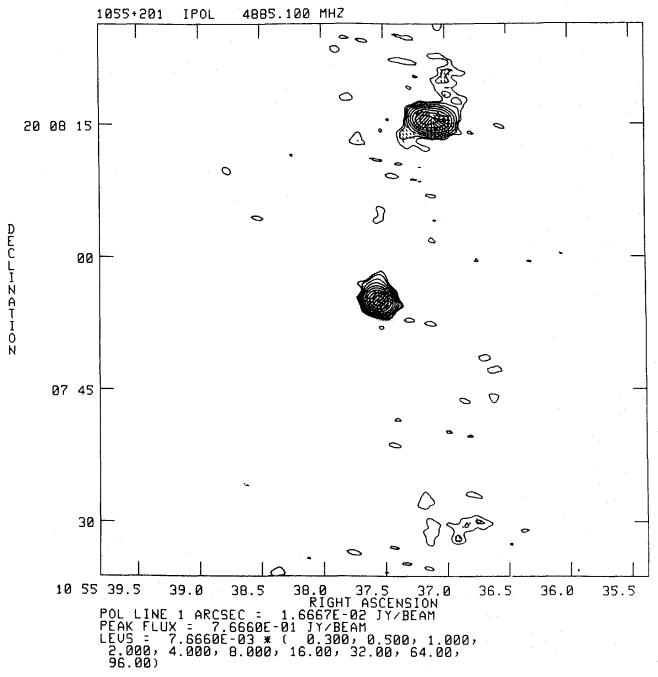

Fig. 2b. VLA map of the total intensity distribution I of 1055+201 at 5 GHz. The contour values in the map are 0.35, 0.5, 1, 2, 4, 8, 16, 32, 64 and 96% of the peak flux value of 766.6 mJy per beam. Superimposed on the contour plot are the electric vectors of the linearly polarized emission P, scaled in length to the intensity of P. An electric vector 1″ in size corresponds to a polarized flux density of 10 mJy per beam

spectrum core ($\alpha_5^{15} \sim -0.4$, using the convention $S_\nu \propto \nu^{-\alpha}$). At 15 GHz, almost all of the flux in the map originates from the core. The emission from the northern lobe is faint; the southern lobe is undetectable. The 15 GHz map is therefore not shown here. At 5 GHz (Fig. 2b), the nucleus of 1055+201 contains ~80% of the total flux density of the source. In the 5 GHz map, slight extensions can be seen to the north of the core and to the south of the northern lobe, but otherwise there is no trace of a large scale radio jet in the 5 and 15 GHz maps.

The bright northern lobe has a complex morphology. In the 5 GHz map of Fig. 2b the lobe emission is clearly resolved in the east-west direction. In our 15 GHz data and in a higher dynamic range 15 GHz map by Owen (private communication), the northern lobe contains a double hot spot structure, the two peaks being linked by a ridge of emission. The surrounding diffuse lobe emission is extended mainly to the north of the two hot spots, away from the core. The hot spot structure and the connecting bridge are oriented nearly perpendicular to the radio source axis. The weak extension to the southeast of the lobe visible in the 5 GHz map suggests that the kpc-scale jet terminates close to the brightest, eastern hot spot. The part of the jet visible in the map in the vicinity of the primary hot spot is linearly polarized at a level of 1%, with the electric vector field running parallel to the jet direction. In the hot spot region the magnetic field becomes circumferential. The primary hot spot has a somewhat higher degree of polarization and flatter spectrum than the secondary, western one. The lobe emission south of the nucleus is diffuse and of low surface brightness. In the low signal-to-noise 1.4 GHz VLA map of 1055+201 published by Hintzen et al. (1983), the southern lobe was not visible, but in deeper 1.4 GHz maps the weak southern emission has been detected clearly (Ulvestad, private communication). In the present 5 GHz map the intensity of the southern lobe emission is barely above the noise level. The linear polarization and the spectral index behaviour of this feature could not be determined with reliability.

3.3. 1222+216

On arcsec scales, this relatively small quasar (with a linear projected radio size of $45h^{-1}$ kpc) possesses a highly distorted triple radio structure (Hintzen et al. 1983; Neff, private communication), with a jet curved over more than 130°. The VLBI map derived from the June 1986 experiment, is shown in Fig. 3. The *uv*-coverage obtained in this observation, was severely limited due to source switching with another source, and to loss of data because of poor tape playback quality. The mas-scale nuclear radio emission consists of a "core–jet"-type structure, oriented nearly north-south, in the direction of the large scale jet. The dominant (~360 mJy) component, A, is assumed to be the radio core; model fitting indicates a secondary component B to be positioned at ~3.3 mas distance, along position angle = −15°, closely aligned with the MERLIN jet (Neff, private communication). A weaker, resolved feature C is present at ~7 mas to the northeast of A. "Missing" flux density on the shortest baselines, unaccounted for by the model, further indicates the presence of some diffuse, extended emission on scales of 20–30 mas, in the region to the northwest of the core.

3.4. 1317+520

(*a*) *Mas-scale radio structure*: On mas scales, the nucleus of this triple quasar displays a curved multi-component radio structure

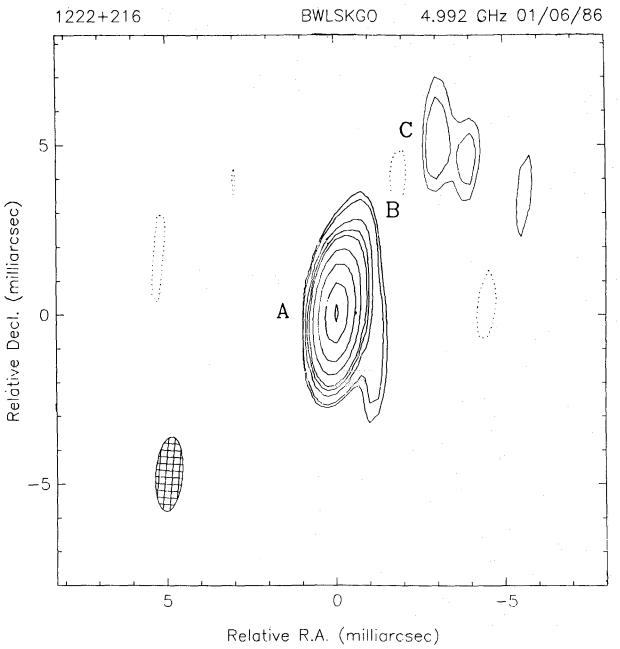

Fig. 3. 5 GHz VLBI map of the total intensity I of 1222+216, observed at epoch 1986.42 in source switching mode with 1055+201. The contour levels in the map are 0.75, 1, 2, 4, 8, 16, 32, 64 and 96% of the peak flux value of 352 mJy per beam. The restoring beam is an ellipse of 3.0 by 0.8 mas, at a position angle of −8°

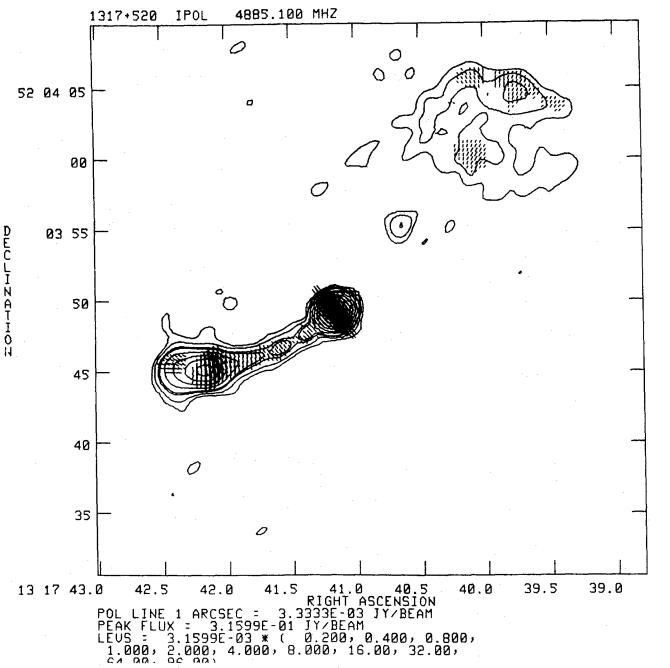

Fig. 4b. VLA map of the total intensity distribution I of 1317+520 at 5 GHz. The contour values in the map are 0.2, 0.4, 0.8, 1, 2, 4, 8, 16, 32, 64 and 96% of the peak flux value of 316.0 mJy per beam. Superimposed on the contour plot are the electric vectors of the linearly polarized emission P, scaled in length to the intensity of P. An electric vector 1″ in size corresponds to a polarized flux density of 3.3 mJy per beam

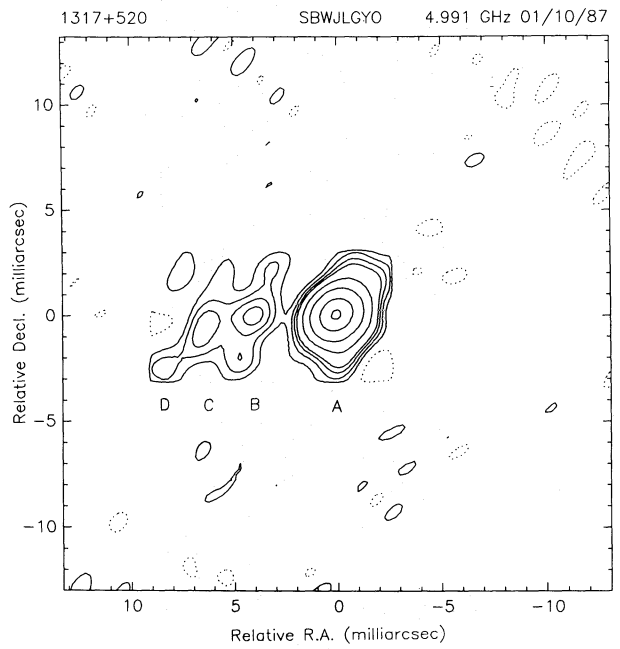

Fig. 4a. 5 GHz VLBI map of the total intensity I of 1317+520, observed at epoch 1987.76. The map has been rotated clockwise over an angle of 35°. The contour levels in the map are 1, 2, 4, 8, 16, 32, 64 and 96% of the peak flux value of 115 mJy per beam. The restoring beam is an ellipse of 1.5 × 0.6 mas, at a position angle of 9°

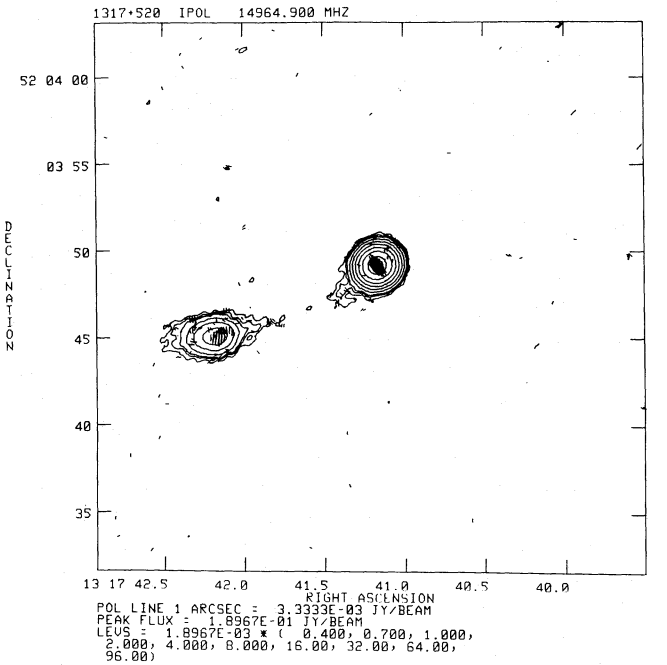

Fig. 4c. VLA map of the total intensity distribution I of 1317+520 at 15 GHz. The contour values in the map are 0.4, 0.7, 1, 2, 4, 8, 16, 32, 64 and 96% of the peak flux density of 190.0 mJy per beam. Superimposed on the contour plot are the electric vectors of the linearly polarized emission P, scaled in length to the intensity of P. An electric vector 1″ in size corresponds to a polarized flux density of 3.3 mJy per beam

(Fig. 4a). At least four separate components, designated A, B, C and D from west to east, can be discerned. Additionally, a small amount of diffuse emission (~ 5 mJy) is present at larger distances (~ 30 mas) from the nucleus.

The brightest, somewhat resolved, component in the hybrid map, A, is assumed to be the core. The mas-scale core–jet structure then is asymmetric in the same sense as the large scale VLA jet (Fig. 4b, c). In view of the possible presence of counterjet emission on kpc scales (see below), an unambiguous spectral identification of the core position by means of VLBI observations at other frequencies is desirable.

The nuclear "jet" curves from east to south; the outer radio jet is seen to curve back again to the east. This morphology is consistent with models involving jet precession.

(*b*) *Large-scale radio structure*: The arcsecond-scale radio structure of 1317+520 is shown in Fig. 4b, c. In the 5 GHz map (Fig. 4b) a bright, continuous jet is seen to extend from the core to the southwest. At $\sim 8''$ from the nucleus, the jet spreads out into a fairly narrow lobe structure, containing a single, intense flux density peak. Both the lobe and the hot spot are elongated in the direction of the slightly curved jet. The hot spot is located at the end of the lobe closest to the radio core. In the 15 GHz map the southern jet emission is very weak, implying a steep radio spectrum for this component: $\alpha_5^{15} \geq 1.5$. At the central knot in the jet $\sim 4''$ from the core the spectrum is slightly flatter ($\alpha = 1.1$) than in its surroundings. The lobe emission has an average spectral index $\alpha_5^{15} \sim 1.0$, the hot spot having the flattest spectrum ($\alpha = 0.7$). The projected magnetic field in the nucleus and the southern jet is directed parallel to the source axis. At 5 GHz the core and the jet are 11 and 3.4% polarized, respectively. At the position of the hot spot, the polarization rises sharply, to 5.9%. The level of polarization is highest on the west side of the hot spot, where the electric vectors are oriented perpendicular to the jet direction. On the east side, the degree of polarization drops sharply, and the magnetic field becomes more circumferential, following the contours of the brightness distribution. In the 5 GHz map, a blob of diffuse emission is present to the northwest of the core. This weak, irregular structure is not detected in the 15 GHz map, and hence of steep spectrum ($\alpha \geq 2.0$). The northern lobe is weakly polarized at 5 GHz; the direction of the magnetic field is circumferential.

The most remarkable feature in the 5 GHz intensity map is the blob of emission located $\sim 5''$ to the northwest of the nucleus, halfway to the northern lobe. The intensity of the northwestern blob is about six times the rms noise level in the 5 GHz map; we therefore believe the feature to be real. The probability of it being an unrelated background source is very small. The position of the blob suggests that it is part of a counterjet extending to the northwestern lobe. This would make 1317+520 a most unusual source, since two-sided jet emission is hardly ever observed in powerful quasars. A peculiar feature of the northwestern blob, however, is its steep radio spectrum: $\alpha_5^{15} \geq 2$, which is unusually high for a knot in a radio jet. It is somewhat mystifying that the blob itself has remained undetected in the 1.4 GHz map of Hintzen et al. (1983), whereas the lobe emission, which at 5 GHz is weaker, is clearly visible at 1.4 GHz. The spectrum of the jet thus should be much steeper than that of the lobe, which is rarely or never observed in quasars. The interpretation of the northwestern blob in terms of counterjet emission therefore remains somewhat doubtful. More sensitive observations of longer duration will be required to settle the issue.

3.5. 1548+114

The optical identification of this radio source is not entirely certain. On photographic plates, two optical objects are visible near the position of the radio nucleus: the close quasar pair 1548+114A (at redshift 0.436) and 1548+114B (at redshift 1.901), located at distances of 2 and 5″ from the radio core, respectively. The QSO closest to the radio nucleus, 1548+114A, has been assumed to be the optical object associated with the radio emission.

(*a*) *Mas-scale radio structure*: The nucleus of 1548+114 is one of the weakest in our sample; it has a flux density close to the limits of mapping with the Mk II recording system. Global fringe fitting has been applied to this source.

The derived VLBI hybrid map of the mas structure is presented in Fig. 5a. Most of the nuclear flux is contained within one slightly resolved component, designated A in the map. A weak secondary feature B is present at ~ 1.5 mas to the northeast of A; but since the flux of B is close to the noise level of the map, its significance is questionable. Another reason to doubt the reality of feature B is the fact that the position angle of B with respect to A differs from that of the large-scale jet of 1548+114 by $\sim 65°$; in most lobe-dominated quasars the arcsec- and mas-scale radio emission tend to be closely aligned. The visibility amplitudes and closure phases on the short and intermediate baselines indicate that there is no resolved structure in the nucleus of 1548+114 on scales larger than 2–3 mas. Due to the low declination of 1548+114, data on the longest baselines cover a small time interval only and do not offer strong constraints on structure within 2–3 mas from the core.

(*b*) *Large-scale radio structure*: At 5 GHz, the radio structure of 1548+114 is double-lobed, with a knotty, straight jet extending

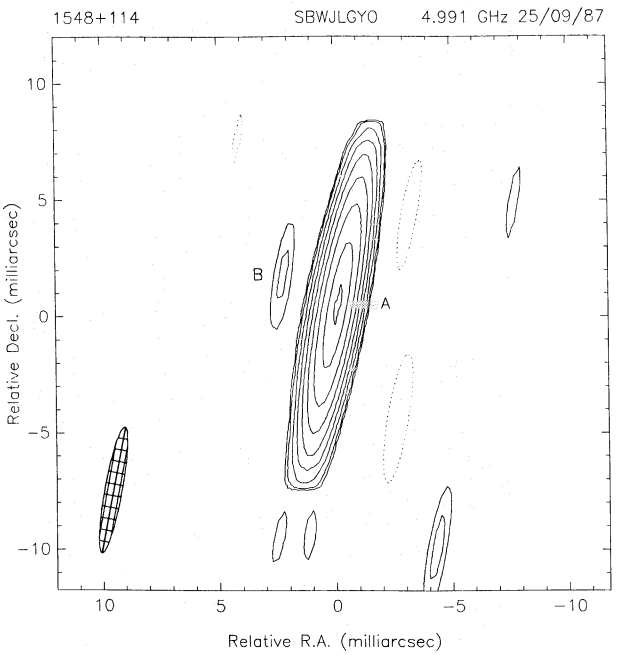

Fig. 5a. 5 GHz VLBI map of the total intensity I of 1548+114, observed at epoch 1987.73. The contour levels in the map are 1, 2, 4, 8, 16, 32, 64 and 96% of the peak flux value of 305 mJy per beam. The restoring beam is an ellipse of 3.5×0.7 mas, at a position angle of $-5°$

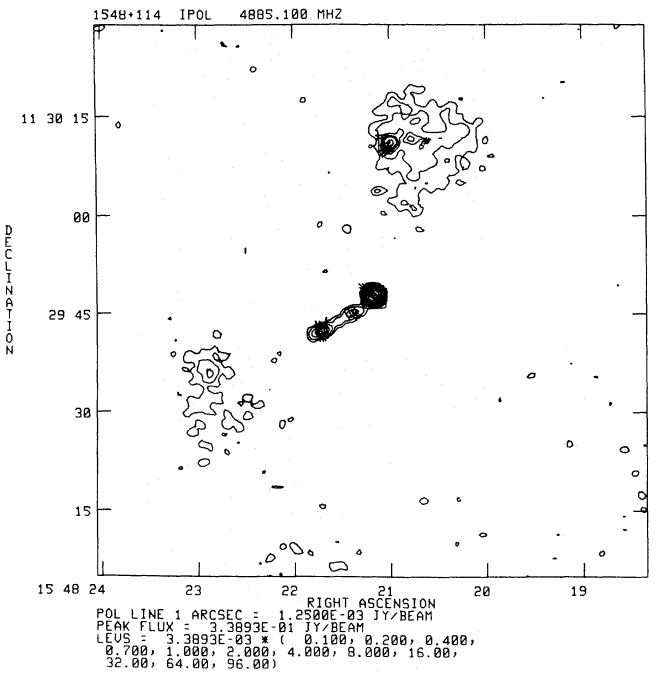

Fig. 5b. VLA map of the total intensity distribution I of 1548+114 at 5 GHz. The contour values in the map are 0.1, 0.2, 0.4, 0.7, 1, 2, 4, 8, 16, 32, 64 and 96% of the peak flux value of 338.9 mJy per beam. Superimposed on the contour plot are the electric vectors of the linearly polarized emission P, scaled in length to the intensity of P. An electric vector 1″ in size corresponds to a polarized flux density of 1.25 mJy per beam

to the southeast of the core (Fig. 5b). The lobe emission is weak and of steep spectrum on both sides of the nucleus. In the 15 GHz map, which is not shown here, there is no detectable jet or lobe emission; the observed intensities imply a flat spectrum for the core ($\alpha = 0.35$), and lower limits for the spectral indices of the jet and the southern and northern lobe (respectively, 1.5, 2.0 and 2.0).

The polarization of the core and southern lobe of 1548+114 in the 5 GHz map is negligible. Only at the two knots in the radio jet and in the northwestern hot spot does the degree of linear polarization rise above the noise level. The projected magnetic field in the jet is oriented parallel to the source axis. In the hot spot the polarization vectors are circumferential.

3.6. 1830+285

(*a*) *Mas-scale radio structure*: The VLBI hybrid map (Fig. 6a) obtained in June 1986 shows the mas-scale emission to have a resolved core–jet morphology. Several components can be distinguished, oriented along a position angle of $-43 \pm 3°$, and aligned with the kpc-scale jet to within 5°. The brightest, eastern component A is assumed to be the radio core. Two other components, designated B and C, are located at distances of 2.1 and 3.9 mas from A, respectively. No emission has been detected to the east of A.

(*b*) *Large-scale radio structure*: The VLA data for this quasar are presented in Fig. 6b, c. Both 5 and 15 GHz maps show a triple structure, with a knotty, discontinuous and slightly curved radio jet leading up to the northwestern lobe. The morphology of this lobe emission is complex (Fig. 6d, e). It contains a bright primary hot spot at the end of the jet and a weaker secondary emission peak to the north. More diffuse emission is also present to the southwest of the primary hot spot. The southeastern radio lobe contains a single central condensation.

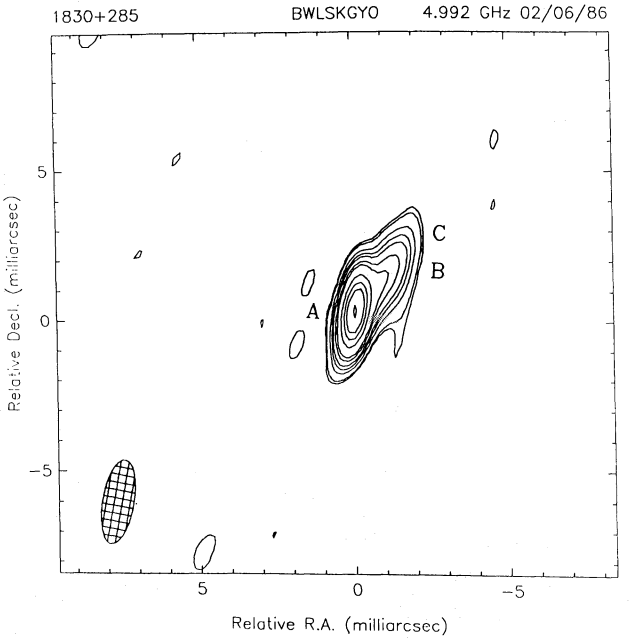

Fig. 6a. 5 GHz VLBI map of the total intensity I of 1830+285, observed at epoch 1986.42. The contour levels in the map are 0.5, 1, 2, 4, 8, 16, 32, 64 and 96% of the peak flux value of 309 mJy per beam. The restoring beam is an ellipse of 2.8 × 1.2 mas, at a position angle of −4°

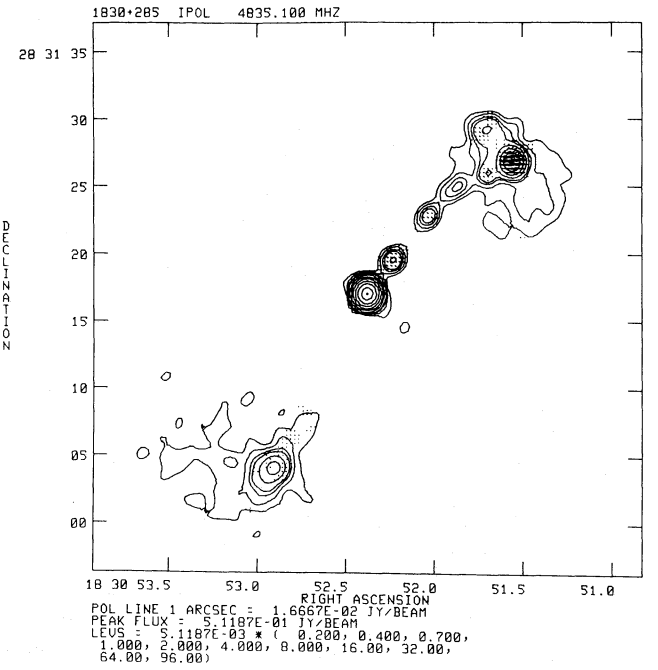

Fig. 6b. VLA map of the total intensity distribution I of 1830+285 at 5 GHz. The contour values in the map are 0.2, 0.4, 0.7, 1, 2, 4, 8, 16, 32, 64 and 96% of the peak flux value of 511.9 mJy per beam. Superimposed on the contour plot are the electric vectors of the linearly polarized emission P, scaled in length to the intensity of P. An electric vector 1″ in size corresponds to a polarized flux density of 16.7 mJy per beam

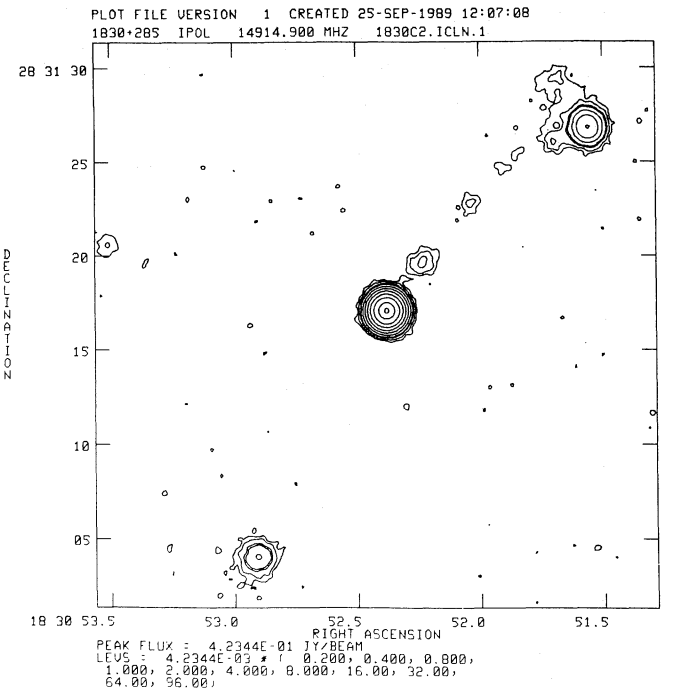

Fig. 6c. VLA map of the total intensity distribution I of 1830+285 at 15 GHz. The contour values in the map are 0.2, 0.4, 0.8, 1, 2, 4, 8, 16, 32, 64 and 96% of the peak flux density of 423.4 mJy per beam

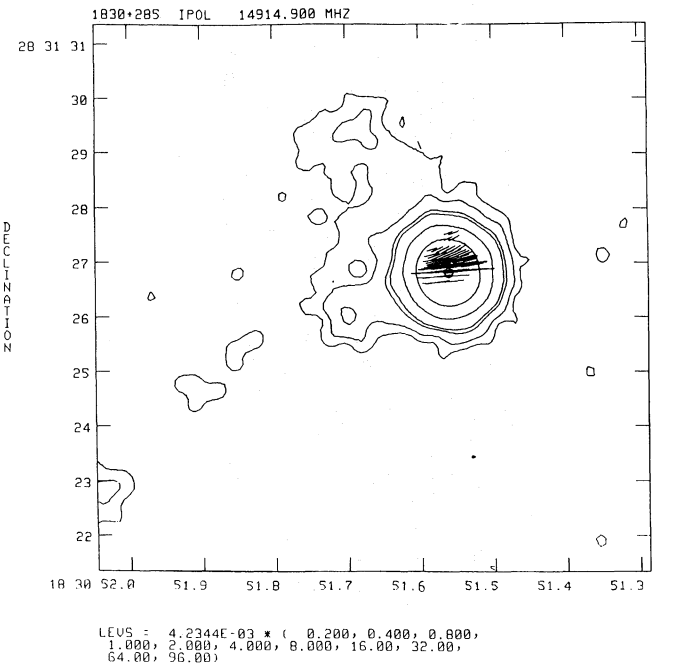

Fig. 6e. The total intensity distribution I and polarization vectors in the north-western hot spot of 1830+285 at 15 GHz. The contour values are the same as in Fig. 6b. A polarization vector 1″ in size corresponds to a polarized flux density of 5.0 mJy per beam

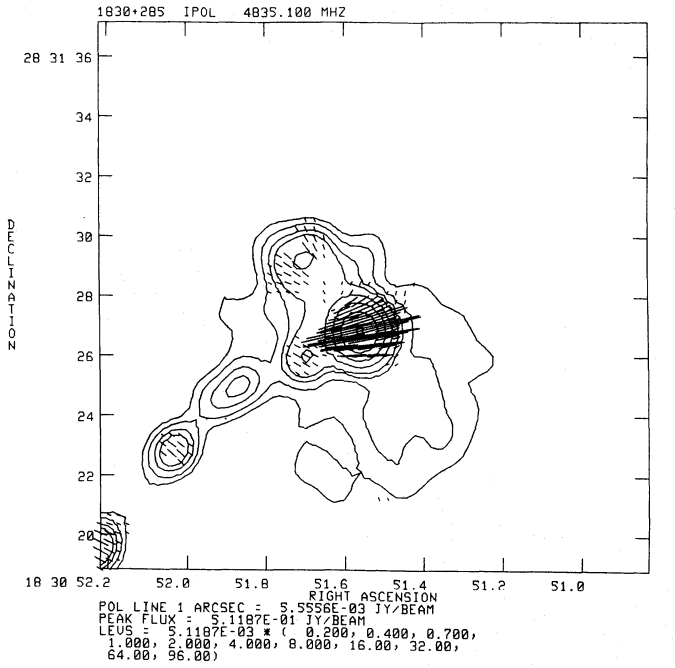

Fig. 6d. The total intensity distribution I and polarization vectors in the north-western hot spot of 1830+285 at 5 GHz. The contour values are the same as in Fig. 6a. A polarization vector 1″ in size corresponds to a polarized flux density of 11.1 mJy per beam

The nucleus of 1830+285 has a fairly flat radio spectrum (α_5^{15} = 0.3), and no significant linear polarization. The one-sided jet structure consists of several knots of emission, forming a curved trajectory between core and primary hot spot. The spectral index of the knots lies in the range 0.5–1.0. The blobs are unresolved in the direction transverse to the jet; but in their longitudinal direction the angular resolution is sufficient to observe a gradient in spectral index over the length of the blobs. In three of the four knots the spectrum within the knots is steepest on the side of the nucleus (0.9–1.0, as compared to 0.5–0.6 on the opposite side). This type of spectral behaviour is predicted in several models of discrete blob emission and of continuous hydrodynamic jets (e.g. Begelman et al. 1984).

The structure of the northwestern lobe has been highlighted in Fig. 6d, e. This region is the only part of 1830+285 which is significantly polarized at either 5 or 15 GHz. Most of the linearly polarized flux is emitted at the location of the primary hot spot. The projected magnetic field in the hot spot is oriented mainly perpendicular to the radio jet axis, at both 5 and 15 GHz.

At 5 GHz, the northern lobe emission contains three substructures: the primary hot spot, the secondary peak to the northwest and diffuse emission to the southwest. In the 15 GHz only the first two features are present; the southwestern emission has a very much steeper spectrum ($\alpha \geq 2.0$). The primary hot spot is unresolved. The ridge of emission between it and the secondary peak is oriented nearly perpendicular to the radio jet, which terminates at the primary hot spot. The observed morphology is suggestive of a redirection of the jet flow at the position of the primary hot spot towards the secondary peak. The flow appears to be deflected over an angle of nearly 120°.

3.7. 2209+080

(*a*) *Mas-scale radio structure*: Snapshot VLBI observations made in October 1984 indicated the presence of resolved structure on mas scales. However, between this epoch and the 6 h

observing run in June 1986, the radio intensity of 2209+080 declined drastically: the total 5 GHz flux density (determined from single-dish measurements by the Effelsberg telescope) dropped by ~40% from 1.1 to 0.85 Jy; the core flux density (defined as the maximum correlated flux density on the shortest VLBI baseline) decreased by ~60% fom 300 to 135 mJy. Much phase noise was present in the 1986 data. Even after application of global fringe fitting, the source remained undetected on most baselines. This suggests that the mas-scale structure of 2209+080 is rather diffuse and extended. To obtain a more reliable map of this radio core in its present low-flux state, use of the more sensitive Mk III recording equipment will be required.

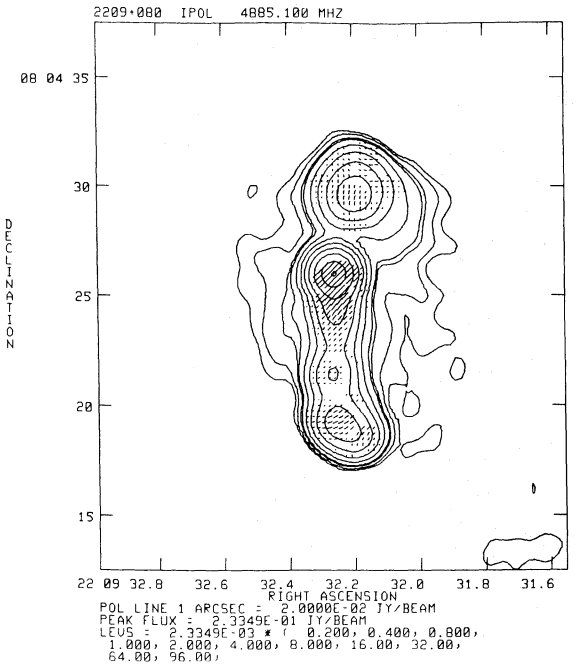

Fig. 7a. The total intensity distribution I of 2209+080 at 5 GHz. The contour values in the map are 0.2, 0.4, 0.8, 1, 2, 4, 8, 16, 32, 64 and 96% of the peak flux value of 233.5 mJy per beam. Superimposed on the contour plot are the electric vectors of the linearly polarized emission P, scaled in length to the intensity of P. An electric vector 1″ in size corresponds to a polarized flux density of 20 mJy per beam

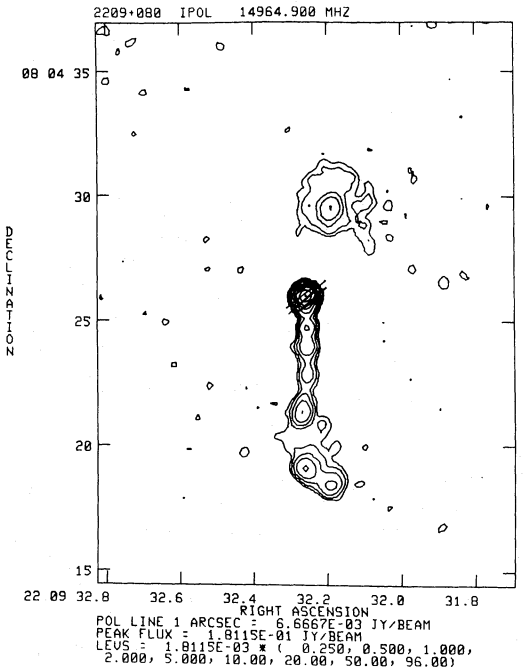

Fig. 7b. The total intensity distribution I of 2209+080 at 15 GHz. The contour values in the map are 0.25, 0.5, 1, 2, 4, 8, 16, 32, 64 and 96% of the peak flux density of 181.2 mJy per beam. Superimposed on the contour plot are the electric vectors of the linearly polarized emission P, scaled in length to the intensity of P. An electric vector 1″ in size corresponds to a polarized flux density of 6.7 mJy per beam

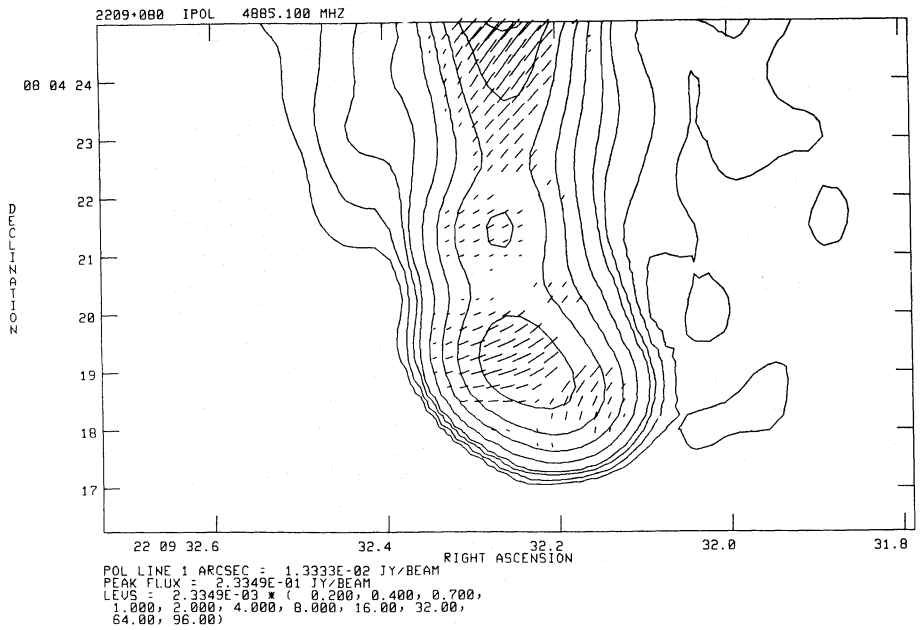

Fig. 7c. The total intensity distribution I and polarization vectors in the southern hot spot of 2209+080 at 5 GHz. The contour values are the same as in Fig. 7a. A polarization vector 1″ in size corresponds to a polarized flux density of 13.3 mJy per beam

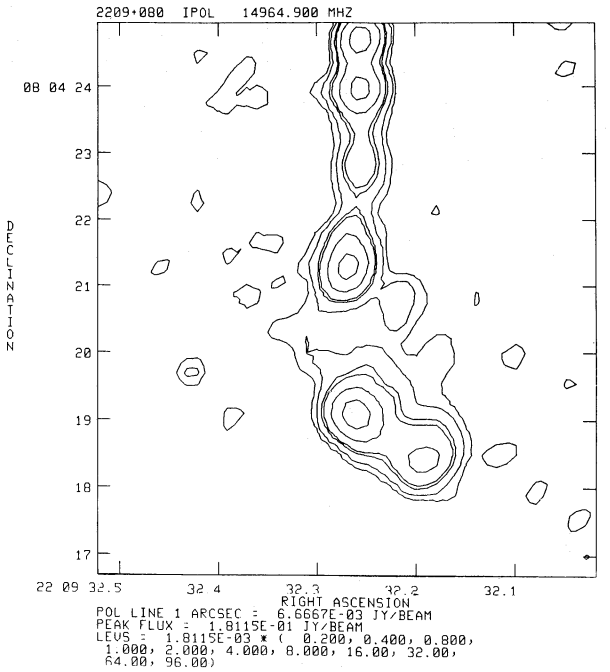

Fig. 7d. The total intensity distribution I and polarization vectors in the southern hot spot of 2209+080 at 15 GHz. The contour levels in the map are 0.2, 0.4, 0.8, 1, 2, 4, 8, 16, 32, 64 and 96% of the peak flux value of 181.2 mJy per beam

(*b*) *Large-scale radio structure*: The radio structure associated with this quasar is shown in Fig. 7a, b. The triple morphology is aligned nearly north-south, with a prominent jet extending to the southern lobe. In the 5 GHz map the southern jet is continuous and fairly smooth; the flux density ratio between the jet and the emission to the north of the core is low (~ 4). The 15 GHz map, on the other hand, shows a strongly asymmetric radio source, with a jet–counterjet flux density ratio ≥ 90, and a considerable amount of structure in the southern jet. The jet emission extends southwards out to a distance of 7″ from the core. At that point it terminates in a double hot spot structure (Fig. 7c, d). The jet is directed towards the brightest, eastern peak. The ridge of emission connecting the primary and secondary hot spots is directed to the southwest, along an angle of 50° with respect to the jet axis. The primary hot spot emission is elongated slightly in the direction of the secondary peak.

At 5 GHz the integrated degree of linear polarization in 2209+080 is 5.6%. Most of the linearly polarized emission is concentrated in the unresolved nucleus. The polarization of jet and lobes is considerably weaker ($\leq 2.0\%$). The electric vectors are oriented mainly along the direction of the radio jet. At 15 GHz the nuclear emission is 1.2% linearly polarized. Outside the core the level of polarization is negligible.

On the whole the spectral index α_5^{15} steepens gradually from the flat spectrum ($\alpha = 0.2$) core along the jet to the southern lobe. The increase in α is not monotonic, since the spectrum flattens noticeably at the positions of the knots in the jet visible in the 15 GHz map. The gradual steepening of the spectrum away from the core is consistent with spectral ageing of the radiating relativistic electrons; the relatively flat spectrum at the positions of the knots in the jet and the two hot spots is an indication of particle reacceleration "in situ" at these points.

As in the case of 1830+285, the morphology and spectral behaviour of the double hot spot structure suggests that, at reaching the primary hot spot, the radio jet has collided with, and been deflected by, dense intervening matter. The abrupt change in direction of the radio emission, the elongation of the primary hot spot towards the secondary, and the steeper spectrum of the secondary are all consistent with this interpretation.

3.8. 2251+134

(*a*) *Mas-scale radio structure*: Full-track VLBI observations of this optically faint quasar were first obtained in September 1985; but since in this experiment no less than four of the eight available stations failed, the source was re-observed in June 1986. In this run, source switching took place between 2209+080 and 2251+134, resulting in a considerable loss of information in the *uv*-plane. The quantity of data was further diminished by the poor playback performance of a number of data tapes. Also, the visibility data do not show clear maxima or minima. The data therefore do not offer enough restrictions to allow an accurate mapping of any structure of great complexity.

The closure phases, which are offset from the zero level, indicate the presence of asymmetric mas-scale radio structure in the nucleus of 2251+134. The cleaned map, displayed in Fig. 8a, shows a resolved, asymmetric three-component structure approximately 4 mas in angular extent. The westernmost, brightest component contains $\sim 75\%$ of the flux on the shortest baselines. The two other components are of nearly equal flux density and positioned at distances of 1.4 and 2.8 mas to the east of the peak flux density position. The three-component "core–jet" structure is aligned to within 10° with the large-scale radio emission. Assuming that the brightest component in the VLBI

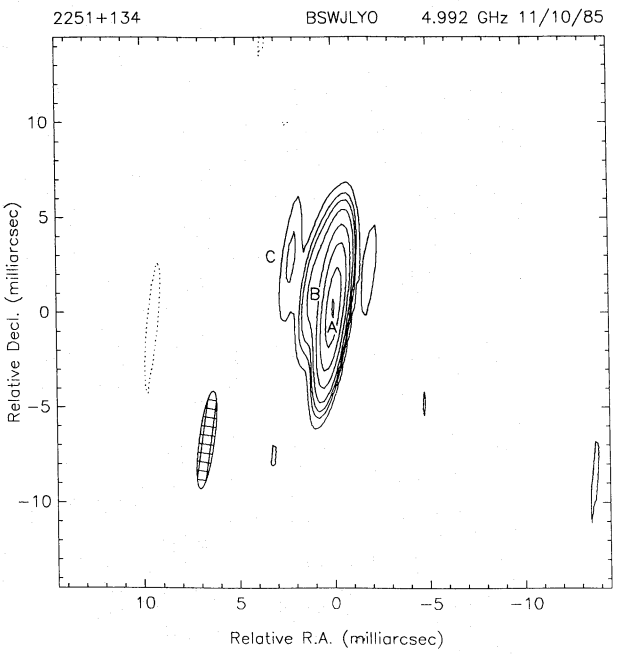

Fig. 8a. 5 GHz VLBI map of the total intensity I of 2251+134, observed at epoch 1986.42. The contour levels in the map are 1, 1.5, 2, 3, 4, 8, 16, 32, 64 and 96% of the peak flux value of 370 mJy per beam. The restoring beam is an ellipse of 4.0×0.6 mas, at a position angle of −5°

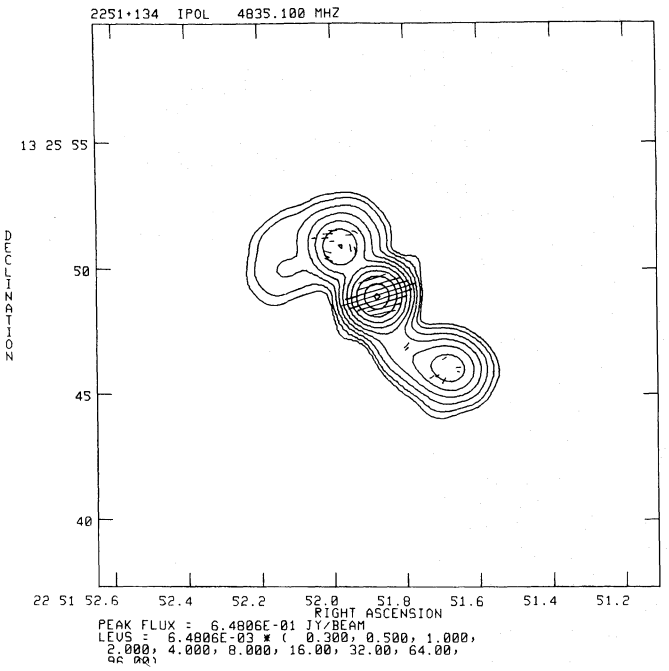

Fig. 8b. The total intensity distribution I of 2251+134 at 5 GHz. The contour values in the map are 0.3, 0.5, 1, 2, 4, 8, 16, 32, 64 and 96% of the peak flux value of 648.1 mJy per beam. Superimposed on the contour plot are the electric vectors of the linearly polarized emission P, scaled in length to the intensity of P. An electric vector 1″ in size corresponds to a polarized flux density of 4.9 mJy per beam

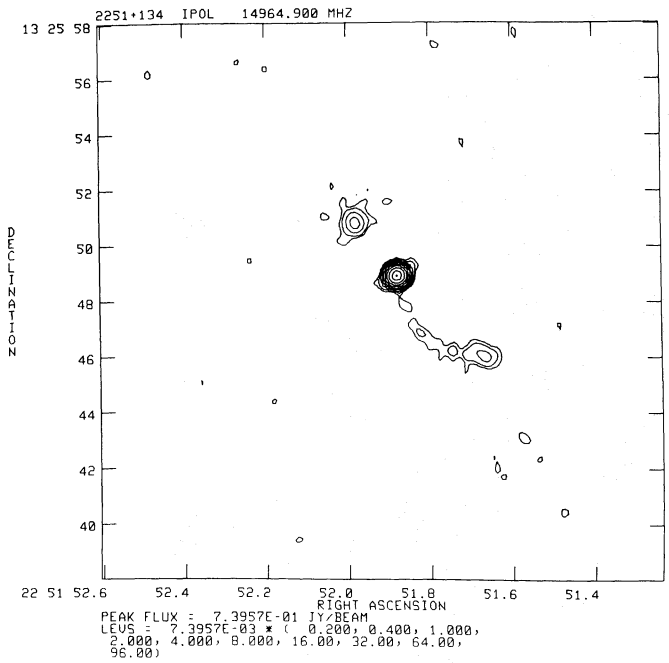

Fig. 8c. The total intensity distribution I of 2251+134 at 15 GHz. The contour values in the map are 0.3, 0.5, 1, 2, 4, 8, 16, 32, 64 and 96% of the peak flux density of 730.2 mJy per beam

map represents the quasar core, the mas-scale jet of 2251+134 is pointing in the direction *opposite* to that of the overall radio morphology (see below). If confirmed, this would make 2251+134 an unusual object among lobe-dominated quasars, in which the mas-scale emission normally is pointing in the same direction as the large scale jet to within a few degrees. VLBI observations at another frequency are required to establish the location of the radio nucleus, and hereby the direction of the VLBI "jet", definitely.

(*b*) *Large-scale radio structure*: The quasar 2251+134 is associated with a relatively small triple radio source (~13″ in angular extent), having a bright, dominant radio core. At 5 GHz (Fig. 8b), the overall morphology is somewhat Z-shaped: the northeastern emission apparently bends rather abruptly through nearly 90° towards the east at a location 2.5″ distant from the core, while the southwestern structure curves more gradually to the west.

The 15 GHz map (Fig. 8c) displays a weak curved jet extending to, and terminating at, the southwestern intensity peak. The spectrum of both jet and lobe emission is rather steep: $\alpha_5^{15} \geq 1.5$. The northeastern emission at 15 GHz consists only of the compact feature 2.5″ away from the core (which has an average spectral index $\alpha \sim 1.0$). The additional structure towards the east that was apparent in the 5 GHz data is not visible here. The absence of the eastern emission in the 15 GHz map implies that the radio spectrum in this region is steep: $\alpha \geq 1.5$. The integrated degree of linear polarization in 2251+134 at 5 GHz is 3.2%. Most of the polarized radiation is emitted by the core; jet and lobes are only marginally polarized. At 15 GHz, the polarized emission was very weak and noisy.

4. Comparison of pc- and kpc-scale radio jets

In all sources except 1055+201 jet emission of kpc-scale dimensions is observable at 5, and sometimes at 15 GHz. The large-scale jet structures usually appear to be one-sided. Only in the case of 1317+520 is there any indication of the presence of counterjet emission above the noise level; but the identification of the feature to the northwest of the core of 1317+520 as being part of a counterjet remains doubtful.

The level of linear polarization at 5 and 15 GHz generally was low, a few percent at most. For the six sources for which polarization maps were derived, the polarized flux densities were too low to permit a determination of the degree of depolarization of the various substructures in the maps.

On mas scales, the nucleus of 1548+114 appears to be unresolved, that of 1055+201 has a symmetric appearance, and that of 2209+080 is too weak to be mapped. The cores of the remaining five quasars, 0850+581, 1222+216, 1317+520, 1830+285 and 2251+134 display an asymmetric core–jet structure similar to the morphologies observed in more core-dominated objects. The nuclear structures in the extended quasars sources usually point in the direction of the kpc-scale radio jet; the elongated nuclear emission is well aligned (to within 10°) with the overall radio morphology. The exception is 2251+134, in which the nuclear emission is directed opposite to the outer jet structure (assuming that the brightest feature in the VLBI map represents the radio core).

Four of the eight quasars possess highly curved or distorted large-scale jets: 0850+581, 1222+216, 1317+520 and 2251+134. For these sources, the behaviour of the nuclear emission on one hand, and the outer radio structure on the other, is consistent with a gradual and continuous bending of the jet from pc to kpc scales. In all objects, the position angles of the secondary VLBI components correspond closely to that of the *inner* part of the kpc-scale jet.

The distorted overall structures of the quasars 0850+581, 1222+216 and 2251+134 suggest that the radio jets in these objects may be precessing. In the highly distorted source 1222+216, the jet bends continuously over an angle of more than 130° from the nucleus to the eastern lobe [compare Fig. 3a to the VLA map of Hintzen et al. (1983)]. In terms of precession models, this high degree of curvature is consistent with a geometry in which the jet axis is inclined close to the line of sight.

In the cases of 0850+581 and 1317+520, the VLBI maps show that the curvature of the radio jet sets in within a few parsecs of the core. The nuclear radio emission of 0850+581 (Fig. 1a) shows a wiggly structure which resembles the "corkscrew" morphology of the large-scale radio jet (Shone 1985; Browne 1987). In 1317+520, the mas-scale "jet" emission appears to bend in a direction opposite to that of the kpc-scale radio jet; this observation lends support to the suggestion that in this source, too, the radio structure may be affected by jet precession.

5. Hot spot emission and jet velocity

The asymmetric jet morphologies generally observed in quasars on both pc and kpc scales are consistent with the presence of relativistic motions throughout the radio jets. In view of the potentially great influence of the velocity of the radio-emitting material on the radiative properties of a source, it is evidently of great interest to obtain independent estimates of the velocities in jets at all length scales. Expansion speeds close to the nucleus are usually estimated from VLBI proper motion studies, although the interpretation of these structural changes on pc scales in terms of material motion is by no means certain. It is more difficult to obtain estimates of the jet velocity closer to the outer lobes. One indirect measure of the order of magnitude of the jet material speed can be obtained from observations of quasar hot spots. Hot spots are believed to be the locations where the radio jet terminates and dumps the bulk of its kinetic energy. Under the assumption of dynamical equilibrium between jet and hot spot, the observed luminosity and energy density of the hot spot emission can be used to place constraints on the velocity of the jet and the momentum carried by it.

Let us consider a situation in which the radio jet is in pressure balance with the hot spot:

$$\rho_j(\gamma_j v_j)^2 = \frac{u_{hs}}{3}, \tag{1}$$

where ρ_j is the jet density in the comoving frame, v_j the velocity of the working surface of the jet at the hot spot position, γ_j the accompanying Lorentz factor and u_{hs} the energy density internal to the hot spot. For u_{hs} we adopt the minimum energy value. The hot spots are assumed to be spherical in shape and uniformly filled. Since the hot spots of all sources observed by us are unresolved, we will assume a typical hot spot radius of 0.1 kpc; VLBI observations of several compact hot spot structures by Lonsdale & Barthel (1984, 1986) have yielded radii of this order of magnitude. We will further assume that the jet deposits its bulk kinetic energy into the hot spot region, where it is converted into radio emission at some efficiency $\varepsilon < 1$. This results in an energy balance of the form

$$L_j = \frac{L_{hs}}{\varepsilon} = \pi r_j^2 \rho_j v_j c^2 \gamma_j(\gamma_j - 1), \tag{2}$$

where L_j and L_{hs} are the kinetic power of the jet and the hot spot radio luminosity, respectively, and r_j is the radius of the jet. Combining Eqs. (1) and (2) and eliminating ρ_j, we find the efficiency of conversion from kinetic to radio energy to be

$$\varepsilon = 3.18\ 10^{-11} \frac{L_{hs}}{u_{hs} r_j^2} \left(\frac{\gamma_j + 1}{\gamma_j - 1}\right)^{1/2}, \tag{3}$$

where the units of L_{hs}, u_{hs} and r_j are 10^{43} erg s^{-1}, erg cm^{-3} and kpc, respectively.

The efficiency factor ε takes into account, among other effects, the fact that a certain fraction of the jet energy is not radiated away at the hot spot position, but gives rise to the diffuse radio lobes. Thus, we essentially adjust for the presence of the lobe emission through the correction factor ε. An alternative approach would be to apply the luminosity and energy density of the entire lobe emission in Eq. (3), rather than the values of L_{hs} and u_{hs} for the hot spot alone. Since for the sources under consideration here the overall lobe emission is dominated by the hot spots, these two methods yield quantitatively similar results. The major source of uncertainty lies in the (unknown) efficiency by which the jet energy is converted into radiation. The accuracy of our estimate for this conversion factor, which is included in ε, determines the accuracy of the jet velocity estimates derived by the model.

A lower limit to the efficiency ε of the energy conversion is obtained by considering the maximum possible values of γ_j and r_j: $\gamma_j = \infty$ and $r_j = r_{hs}$. For the three quasars in our sample having the most pronounced hot spot emission (1055+201, 1830+285 and 2209+080), the calculated values of ε_{min} range between 0.01 and 0.15 (Table 5).

Assuming a maximum efficiency ε of 1, Eq. (3) yields a lower limit to γ_j and v_j. For the three sources involved, minimum jet velocities ranging from 0.33 to 0.65c are obtained. Actually, the maximum possible value of ε is likely to be well below unity, as not all of the kinetic energy will be converted to radiative energy. Thus, the given lower limits to v_j are probably underestimates. Gopal-Krishna & Saripalli (1984) argue that a reasonable upper limit for ε in powerful double radio sources is given by $\varepsilon_{max} = 0.3$. Using this value, we derive minimum jet velocities ranging from 0.57 to 0.92c (Table 5).

On the basis of this simple model, therefore, we conclude that, close to the hot spots, the flow velocities of the quasar jets are relativistic. In extended quasars with bright radio cores, such as the ones studied here, highly relativistic motion is commonly detected on mas scales (Impey 1987; Cohen et al. 1988). Depolarization measurements by e.g. Garrington et al. (1988) and Laing (1989) indicate that the jets in these objects are likely to retain most of their kinetic energy as far out as the radio lobes. One would therefore expect to find relativistic motions in the hot spot

Table 5. Physical parameters of hot spot sources

Source	1055+201	1830+285	2209+080
u_{hs} (10^{-9} erg cm^{-3})	9.9	2.4	0.9
L_{hs} (10^{43} erg s^{-1})	2.2	1.0	0.8
ε_{min}	0.07	0.13	0.03
γ_{min} ($\varepsilon_{max} = 1$)	1.15	1.30	1.06
β_{min} ($\varepsilon_{max} = 1$)	0.49	0.64	0.33
γ_{min} ($\varepsilon_{max} = 0.3$)	1.60	2.5	1.22
β_{min} ($\varepsilon_{max} = 0.3$)	0.78	0.92	0.57

regions of superluminal triple quasars. The kinematical model presented here, however crude, is consistent with this prediction.

6. Discussion

In the context of a study of the structural evolution within the nuclei of large double-lobed quasars, we have obtained first epoch VLBI maps of eight quasars with extended radio structure. For five of the eight sources shown here, the VLBI data yielded maps of good quality. In one quasar, 2209+090, the core flux density at the time of observation had dropped below the level at which Mk II observations can produce reasonable signal-to-noise maps. For two other sources, the quasars 1055+201 and 2251+134, the data were of low quality due to a large loss of data and a consequently inadequate *uv*-coverage.

The most well-known source in our sample is the quasar 0850 +581, for which Barthel et al. (1986) have reported the occurrence of superluminal motion. Our 5 GHz map confirms the structure and expansion velocity found by Barthel et al. Clear multi-component structure was detected in the nuclei of 1222+216, 1317+520 and 1830+285 as well. The relative flux densities of the nuclear components in these objects indicate that the mas-scale radio emission is one-sided. In the quasar 1548+114 no resolved nuclear radio emission was detected, in contrast to expectations based on an earlier pilot survey (Barthel et al. 1984). Of the two sources with low quality VLBI maps, 1055+201 is a candidate source for symmetrical nuclear structure, while 2251 +134 appears to have a more conventional core–jet morphology.

The multi-component structures present in five of the observed extended quasars designate these sources as candidates for proper motion studies. The nuclei of the quasars 1222+216 and 1830+285 have later been reobserved at 5 GHz. Indications for the presence of superluminal motion were found in both cases (Hooimeyer et al. 1991); mapping at a third epoch is required to confirm the observed proper motion values. The nuclei of the sources 1317+520 and 2251+134 have not yet been re-observed. Because of its multi-component nuclear structure, the former is a good candidate for further VLBI monitoring. The nucleus of 1317 +520 is at the lower edge of the flux density range for which Mk II observations yield reliable maps; it would therefore be preferable to perform future VLBI observations of this source with Mk III networks.

In all, VLBI monitoring of the 13 extended quasars in our sample for which the initial pilot surveys (Barthel et al. 1984, HBSM) indicated the presence of resolved nuclear emission, has led by now to three confirmed cases of superluminal motion: 0850 +581 (Barthel et al. 1986), 1137+660 (Hough & Readhead 1987) and 1721+343 (Barthel et al. 1989; Hooimeyer et al. 1991). In two other candidates, 1222+216 and 1830+285, the observed proper motions indicate superluminal velocities (Hooimeyer et al. 1991), but these results remain to be confirmed. The observed velocities in all cases are in the range of 1–3*c*, moderate values compared to those found in more core-dominated objects.

VLA observations were made for six of the eight lobe-dominated quasars at 5 and 15 GHz. Polarization images and spectral index maps were obtained for most objects. Energy density, magnetic field strength and velocity estimates were derived for the various components in each source. The misalignment between the nuclear emission and the inner part of the kpc-scale radio jet is small in all cases except 2251+134, where the VLA and VLBI jets appear to be oppositely directed. The overall structure of the distorted sources 0850+581, 1222+216 and 2251 +134 is suggestive of precession of the radio jet. A comparison between the curved emission on pc and kpc scales in the quasar 1317+520 shows that the morphology of this source is compatible with precession models as well.

In several sources a well-defined, sometimes double, hot spot structure was present. The kinematical model of this hot spot emission described in Sect. 5, implied relativistic motions to be present in those regions. Within the context of the simple relativistic beaming model, the inferred high velocity values are consistent with the jet–counterjet flux density asymmetric observed on kpc scales; they are in conflict, however, with the symmetric appearance of the lobe structure (in terms of both flux density and separation from the core) in these lobe-dominated quasars.

In roughly 1/3 of the large double quasars under consideration here, evidence for moderately superluminal expansion was found, implying the presence of relativistic motions close to the quasar nuclei. Observations of lobe-dominated quasars from other samples (e.g. Hough & Readhead 1987, 1989; Zensus & Porcas 1986) yield similar results. The superluminal expansion velocities detected in a large fraction of the lobe-dominated quasars that have been monitored to date, imply these objects to be inclined at relatively small angles to the line of sight, in spite of their large projected radio sizes. If the sources for which proper motions have been determined so far are representative for the quasar population as a whole, then the simple relativistic beaming model as formulated by Orr & Browne (1982) is clearly inconsistent with the data. A better agreement with the observations is then obtained by a modified version of the beaming model, in which quasars are proposed to be powerful double-lobed radio galaxies inclined close to the line of sight (Scheuer 1987; Barthel 1989).

Nevertheless, one should keep in mind that the observations available at present give us an incomplete, and possibly highly misleading, picture of the distribution of apparent velocities in quasar nuclei. The few double-lobed quasars that have been studied in detail, all possess relatively bright radio cores. The double-lobed quasars with truly weak nuclear radio emission, in which subluminal motion is much more likely to occur, and far more difficult to observe, and may not be accessible to VLBI networks for some time. Also, many lobe-dominated sources have simply not yet been monitored sufficiently long to definitely establish proper motions. At the presently attainable resolutions, the detection of subluminal motion in an intermediate redshift ($z \sim 0.5$–1.0) quasar requires a monitoring period of 10 yr or more; few lobe-dominated sources have been studied this long. The observed distribution of apparent velocities is therefore subject to a heavy bias against the inclusion of subluminal sources. It is significant that, as time has progressed, ever lower apparent velocities have been detected in ever weaker nuclei. Patient monitoring of weak radio cores might well reveal the presence of a large population of subluminal quasars, which hitherto has been impossible to detect.

With the coming of age of the very large baseline array (VLBA), routine monitoring of large samples of objects with relatively weak radio cores over a period of 10 yr or more, has become a possibility. An observing program dedicated to this purpose, however unspectacular and lacking results in the short run, will provide us with essential information on the true

distribution of apparent velocities in quasar nuclei and should be given high priority.

Acknowledgements. We thank the staff at the telescopes involved in this experiment for their assistance with the observations, and the correlator staff at the California Institute of Technology for their help with the data processing. We gratefully acknowledge the assistance of Joris Blommaert in the reduction of the data. The NRAO VLA is operated by Associated Universities Inc., under contract with the National Science Foundation. The Netherlands Foundation for Research in Astronomy is supported by the Netherlands Organization for Scientific Research (NWO).

References

Barthel P.D., 1987, in: Pearson T.J., Zensus J.A. (eds.) Superluminal Radio Sources. p. 148
Barthel P.D., 1989, ApJ 336, 606
Barthel P.D., Miley G.K., Schilizzi R.T., Preuss E., 1984, A&A 140, 399
Barthel P.D., Miley G.K., Schilizzi R.T., Preuss E., 1985, A&A 151, 131
Barthel P.D., Pearson T.J., Readhead A.C.S., Canzian B. 1986, ApJ 310, L7
Barthel P.D., Hooimeyer J.R., Schilizzi R.T., Miley G.K., Preuss E., 1989, ApJ 336, 601
Begelman M.C., Rees M.J., Blanford R.D., 1985, Rev. Mod. Phys. 56, 255
Blandford R.D., Königl A., 1979, ApJ 232, 34
Browne I.W.A., 1987, in: Pearson T.J., Zensus J.A. (eds.) Superluminal Radio Sources. p. 129
Cohen M.H., Moffet A.H., Romney J.D., Schilizzi R.T., Shaffer D.B., Kellermann K.I., Purcell G., Grove G., Swenson G., Yen J.H., Pauliny-Toth I.I.K., Preuss E., Witzel A., Graham D., 1975, ApJ 210, 249
Cohen M.C., Barthel P.D., Pearson T.J., Zensus J.A., 1988, ApJ 333, 9
Garrington S.T., Leahy J.P., Conway R.G., Laing R.A., 1988, Nat 331, 147
Gopal-Krishna, Saripalli L., 1984, A&A 141, 61
Hewitt A., Burbidge G., 1980, ApJS 43, 57
Hewitt A., Burbidge G., 1987, ApJS 63, 1
Hintzen P., Ulvestad J.S., Owen F.N., 1983, AJ 88, 709
Hooimeyer J.R.A., Barthel P.D., Schilizzi R.T., Miley G.K., 1991, ApJ (submitted) (HBSM)
Hough D., Readhead A.C.S., 1987, ApJ 321, L11
Hough D., Readhead A.C.S., 1989, AJ 98, 1208
Impey C., 1987, in: Zensus J.A., Pearson T.J. (eds.) Superluminal Radio Sources, p. 233
Laing R.A., 1989, in: ESO Workshop, Extranuclear activity in galaxies. p. 52
Lonsdale C., Barthel P.D., 1984, A&A 135, 45
Lonsdale C., Barthel P.D., 1986, AJ 92, 1
Miley G.K., 1980, ARA&A 18, 165
Neff S.G., Brown R.L., 1984, AJ 89, 195
O'Dea C., Barvainis R., Challis P.M., 1988, AJ 96, 435
Orr M.J.L., Browne I.W.A., 1982, MNRAS 200, 1067
Owen F.N., Puschell J.J., 1984, AJ 89, 932
Pearson T.J., Readhead A.C.S., 1984, in: Fanti R., Kellermann K.I., Setti G. (eds.) Proc. IAU Symp. 110, VLBI and compact radio sources. p. 15
Scheuer P.A.G., 1984, in: Fanti R., Kellermann K., Setti G. (eds.) Proc. IAU Symp. 110, VLBI and compact radio sources. p. 197
Scheuer P.A.G., 1987, in: Zensus J.A., Pearson T.J. (eds.) Superluminal Radio Sources. p. 104
Scheuer P.A.G., Readhead A.C.S., 1979, Nat 277, 182
Schwab F.R., Cotton W., 1983, AJ 88, 688
Shone D., 1985, Ph.D. Thesis, Univ. of Manchester
Thompson A.R., Clark B.G., Wade C.M., Napier P.J., 1980, ApJ 44, 151
Zensus J.A., Porcas R.W., 1986, Swarup G., Kapahi V.K. (eds.) Proc. IAU Symp. 119, Quasars. p. 158